Engineering and Technology Journal
Journal homepage: https://etj.uotechnology.edu.iq

Control system design of a Pin-on-Disc wear machine using PLC

Huda J. Mohammed*, Khansaa D. Salman Abed, Ahmed H. Reja

Electromechanical Engineering Dept., University of Technology-Iraq, Alsina'a street, 10066 Baghdad, Iraq.
*Corresponding author Email: Hudaaljumaili7680@gmail.com

HIGHLIGHTS

- Variable applied pressure to the pin improved the wear rate by 2% over the traditional method in an intelligent design.
- Additional development and compression testing were done because the operating system and components are open-source.
- The control system used an HMI and PLC to monitor load, temperature, rotating speed, and friction force.
- The coefficient of friction, specific wear rate, and temperature were determined.
- Wear tests varied factors like rotating speed (300-900 rpm) and applied load (5-25 N).

ARTICLE INFO

Handling editor: Mohammed Y. Hassan

Keywords:
Pin-on-Disc; PLC; Touch screen; AA6061 alloy; CK45 steel alloy.

ABSTRACT

This study presents the design and implementation of a control system for a Pin-on-Disc wear testing machine using a Programmable Logic Controller (PLC). The novel approach employed involves adjusting the applied pressure on the pin, rather than the conventional method of altering weights, to evaluate the impact of varying loads on the wear rate. This method enhanced the accuracy of wear results by 25% compared to traditional techniques. The control system was developed and implemented with a Human-Machine Interface (HMI) that interacts with the PLC to control and monitor key parameters, including applied load, temperature, rotational speed, sliding time, and friction force. Key wear parameters such as the coefficient of friction (COF), wear rate, and temperature were calculated. The wear tests were conducted under varying conditions, with rotational speeds ranging from 300 to 900 rpm, applied loads from 5 to 25 N, and sliding times from 5 to 25 minutes. The results indicated that an increase in applied load led to higher wear rates and temperatures, while the COF decreased. Conversely, an increase in rotational speed reduced the wear rate but increased both the COF and temperature. Prolonged sliding time resulted in higher wear rates and temperatures, while the COF decreased. Additionally, it was observed that the wear rate of the aluminum alloy AA6061 was higher than that of the CK45 steel alloy. The study utilized various software tools, including AutoCAD 2018, SoMove AC Drive Software, EcoStruxure Machine V1.2 VP1, Vijeo Designer 6.2, Ifs – Conf RTD, and MATLAB.

1. Introduction

Wear is the gradual loss of material at solid surfaces due to damage. Wear can have two cases: mechanical (erosion) and chemical (mechanical corrosion) [1]. Dry wear refers to various dynamics involving two sliding bodies and the resulting material loss. Dry wear found in dry clutches, brakes, non-lubricated plain bearings, and other materials is typically categorized as either adhesive or abrasive [2]. Pin-on-disc tests are employed to characterize friction. The pin in this study is loaded against a disc rotating at a certain speed. There is complete control over both sliding speed and normal pressure. Various materials can be examined in an extensive range of speeds and applied load values using very versatile pin-on-disc tests [3]. Tribological tests involving pin-on-disc are frequently employed to study the wear behavior of materials in contact with sliding motions [4]. A pin specimen is usually spherical or cylindrical. The diameters of typical spherical pin or cylindrical specimens vary from 2 to 10 mm. Typically, disc specimens have thicknesses between 2 and 10 mm and diameters between 30 and 100 mm. Usually using an arm with attached weights, at a preset load, the pin specimen is pressed up against the disc [5].

Several studies dealt with the issue of designing and manufacturing the pin-on-disc wear machine such as Matteo Federici et al. presented a model of the surface contact temperature in this sliding system to highlight the role of the different surface conditions, i.e., coated and uncoated, on the evolution of the pin and disc temperatures during sliding [6]. Sobarad et al. [7], designed and fabricated a pin-on-disc wear testing machine, which is used to determine the wear of a given sample. It can determine the wear rate of materials such as Copper, Brass, and aluminum. The machine showed results that were very close to the standard wear rates. Further, the machine can handle different load and speed levels. Gonçalves et al. [8], presented the design

http://doi.org/10.30684/etj.2024.150091.1756
Received 22 May 2024; Received in revised form 11 July 2024; Accepted 30 July 2024; Available online 26 August 2024
2412-0758/University of Technology-Iraq, Baghdad, Iraq

and fabrication of a pin/ball on disk type tribometer, seeking to determine using experimental tests and analysis of material properties, the coefficients of friction, and the wear volume of certain pairs of engineering materials. Ali [9] also gave information about the design steps and manufacturing procedure for the pin-on-disc apparatus and discussed the problems following the design and manufacturing process. The results of the wear testing obtained by the apparatus that has been designed and manufactured show that the test sample's wear increases as the motor's speed (rpm) increases. Also, as the sliding distance increases, the wear decreases at constant load and speed.

The primary distinction between the proposed work and previous studies lies in the novel approach of varying the applied load on the sample. This method involves adjusting the applied pressure, rather than the conventional technique of altering weights, to assess the impact of load changes on the wear rate. Additionally, this design is capable of determining key parameters, including the coefficient of friction (COF), specific wear rate, and temperature. All parameters are also controlled using an HMI screen. Using a PLC and HMI screen resulted in ease of use and speed in wear tests on metal alloys, so the process became 75% faster than the non-programmed wear machine used in previous studies.

The main aim of this work is the design and manufacturing of a control system with a programmable design and production capable of handling loads up to 25 N without the user's intervention in changing the factors affecting the wear rate by changing the values using a Human-Machine Interface (HMI) screen. This screen became the input and output for the device, which led to ease of use and more accuracy in the results. The control system was designed and implemented using HMI, which interacts with input/output sensors, and a Programmable Logic Controller (PLC), which controls and monitors elements such as applied load, temperature, rotating speed, and friction force. There is an opportunity for additional development and compression testing because the operating system and electronic components are open-source.

2. Wear parameters

The various parameters that interact and influence the wear behavior of the prepared samples are illustrated in Table 1. Every parameter's impact is examined in this work.

Table 1: Wear test parameters with their range

Factors	Range				
Load (N)	5	10	15	20	25
Rotating Speed (rpm)	300	450	600	750	900
Sliding Time (min)	5	10	15	20	25

3. Wear measurement

Volume loss, weight loss, geometric measures, and wear scar depth are common methods for measuring wear. Wear measurements can be performed using microscopy methods like Scanning Tunneling Microscopy (STM) and Scanning Electron Microscopy (SEM) [10]. In this work, the weight loss method was used to calculate the wear rate by calculating the weight of the sample before and after testing the device and then applying Archard's wear equations. It is widely accepted in tribology and is arguably the most basic empirical model of wear [11].

The wear rate of each sample is measured using the weighting method, and then Archard wear Equations for abrasive wear are applied as shown in Equations 1, 2, and 3.

$$WR = \Delta w/SD \tag{1}$$

$$SD = 2\pi rnt \tag{2}$$

$$\Delta w = w_1 - w_2 \tag{3}$$

where WR is the wear rate (g/cm), Δw is the weight change, w_1 is the weight of the sample before testing (g), w_2 is the weight of the sample after testing (g), SD is the sliding distance, r is the distance between the sample center and the disc center (cm), n is the number of rotating discs (rpm), and t is the rotating time (min) [12].

4. Coefficient of friction

The force opposing the motion of the friction force (F_f) divided by the applied normal force (F_n) is known as the coefficient of friction, as shown in Equation 4 [13]. It is a dimensionless parameter, which means that the physical matter does not change according to the direction of the force [14].

$$\mu = \frac{F_f}{F_n} \tag{4}$$

The coefficient of friction value is derived from the weight of the object and the way the two in contact surfaces interact, the dynamic forces involved in relative movement, the surface finishes, and the kind of material in contact [15]. Normal and friction force measurements are necessary for calculating the Coefficient of Friction (COF). Figure 1a shows where load cells measure

the normal forces and friction. In this configuration, the orientation of the load cells is determined by the disc surface, and the reaction forces are equal to the interfacial forces between the disc and the ball as shown in Figure 1b.

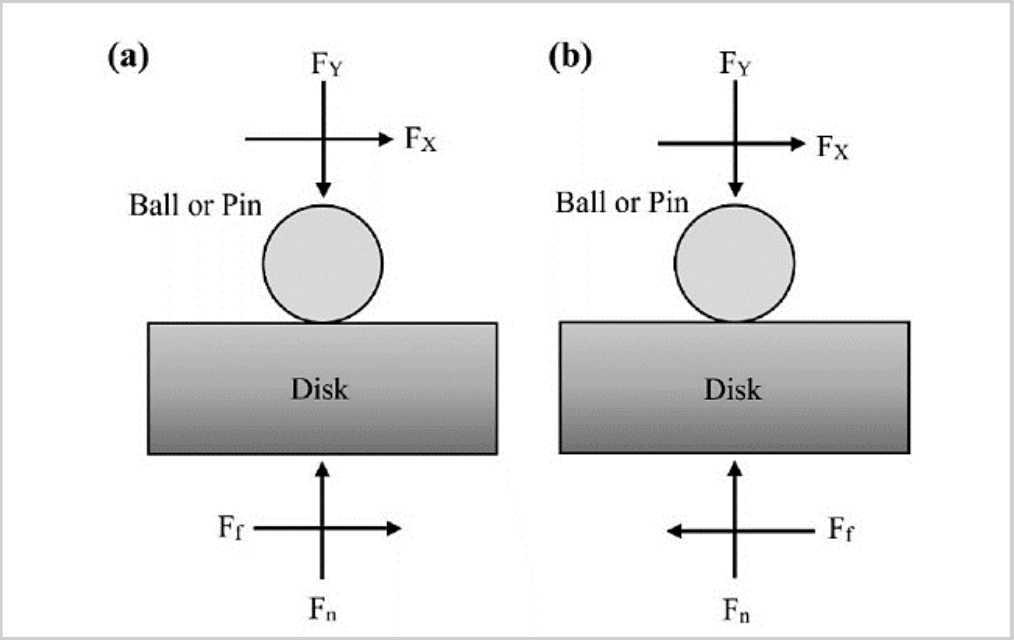

Figure 1: Coefficient of friction measurement: (a) forward sliding, (b) reverse sliding [15]

The measured coefficient of friction (μ') is defined as the ratio of the load cell forces. The load cell forces and the measured friction coefficient (μ') are computed using Equations 5 to 7 utilizing a static equilibrium condition and the definition of the interfacial friction coefficient (μ) [16].

$$F_x = F_f \tag{5}$$

$$F_y = F_n \tag{6}$$

$$\mu' = \frac{F_x}{F_y} \tag{7}$$

The path of forces during the friction analysis is shown in Figure 2. The pin is loaded (W), and the disc rotates at a constant angular speed (ω). The torsion over the disc is denoted as F_{app}, and its rate is equal to F_t. The path taken by static friction force Fc is the opposite one. The net force F_{Net} is what separates Ft from Fc. The tangential force represents the force of dynamic friction. F_{tf} and net force F_{Net}. Equations 8 to 13 demonstrate that the net force is equal to the tangential force [16].

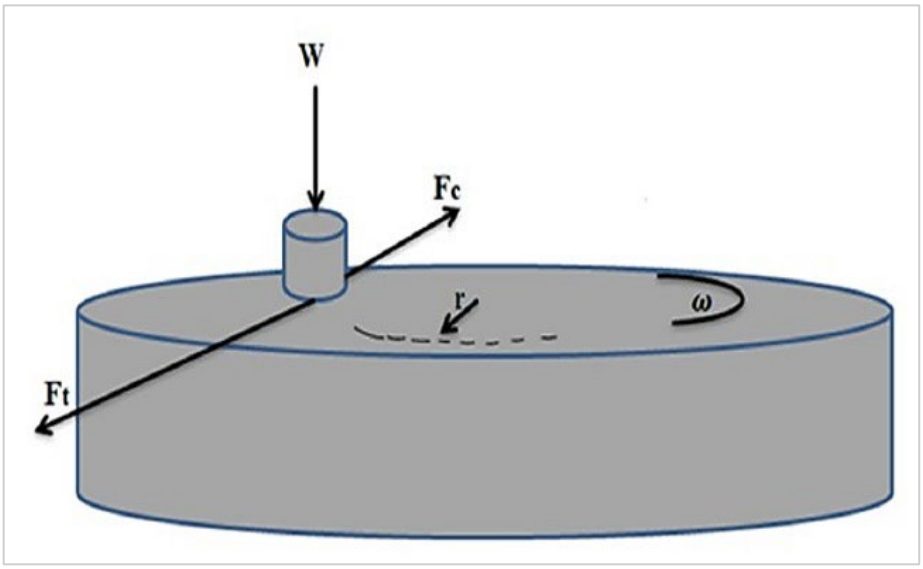

Figure 2: Forces operating in the pin-on-disc test [16]

$$F_t = F_{app} \quad (8)$$

$$F_c = \mu_s W \quad (9)$$

$$F_t - F_c = F_{Net} \quad (10)$$

$$F_{Net} = \mu_d W \quad (11)$$

$$F_{Net} = F_{tf} \quad (12)$$

$$\mu = \frac{F_{tf}}{W} \quad (13)$$

5. Programmable logic controllers (PLCs)

PLCs are an essential part of manufacturing and process industries for compact size, are applied to programming using ladder logic, and permit extensive control and communication between machines and operators. The input and output pins/terminals (digital/analog) on PLCs available today are specifically designated for communication [17].

Figure S1 as shown in the supplementary file depicts a typical PLC architecture. The three primary components of a typical PLC are the input/output controller, memory, and Central Process Unit (CPU) as shown in Figure S2. A bus system connects these blocks and is connected to an external network controller [18,19]. The user PLC program can be created in five different programming languages: Ladder Logic Diagram (LAD), Function Block Diagram (FBD), Structured Control Language (SCL), Structured Text Language (STL), CHART, and GRAPH. In this work, the Ladder Logic Diagram (LAD) language is used [18, 20].

5.1 Ladder logic diagram

An example of a programming language used with PLCs is a Ladder Logic Diagram (LAD). Ladder logic describes hard-wired control using components that look a lot like line diagram elements. An activated left power rail is part of a LAD program, as seen in Figure S3 in the supplementary file. Energy can pass through closed contacts and onto the next element, while open contacts prevent this energy from passing [21].

6. Experimental work

6.1 Design materials

The test samples (pins), including choosing the type of metal. Two types of metals were chosen (AA6061 and medium carbon CK45 steel alloy). This part also includes manufacturing samples based on the specifications of ASTM-G99 and testing the chemical composite and mechanical properties of each metal. Ten samples (pins) were manufactured for each type of metal because two variables will affect the wear rate. Each variable will have five cases, as shown in Table 1.

The pins are prepared with a 12 mm diameter for the upper part for sample fixing, a 10 mm diameter for the lower part for sample testing, and a 46 mm length, as shown in Figure 3. The consideration of ferrous (CK45 steel alloy) and non-ferrous metal (AA6061 alloy) choose the material.

Figure 3: Test pins for two types of metal alloys

The main components of the control system are the emergency switches, sensors, and proximity switches. They send a signal to the PLC, which generates the proper output to the pulley, coupling, and direct motor based on these input signals and the implemented code. Figure 4 provides a general overview of a closed-loop control system that controls electromechanical devices.

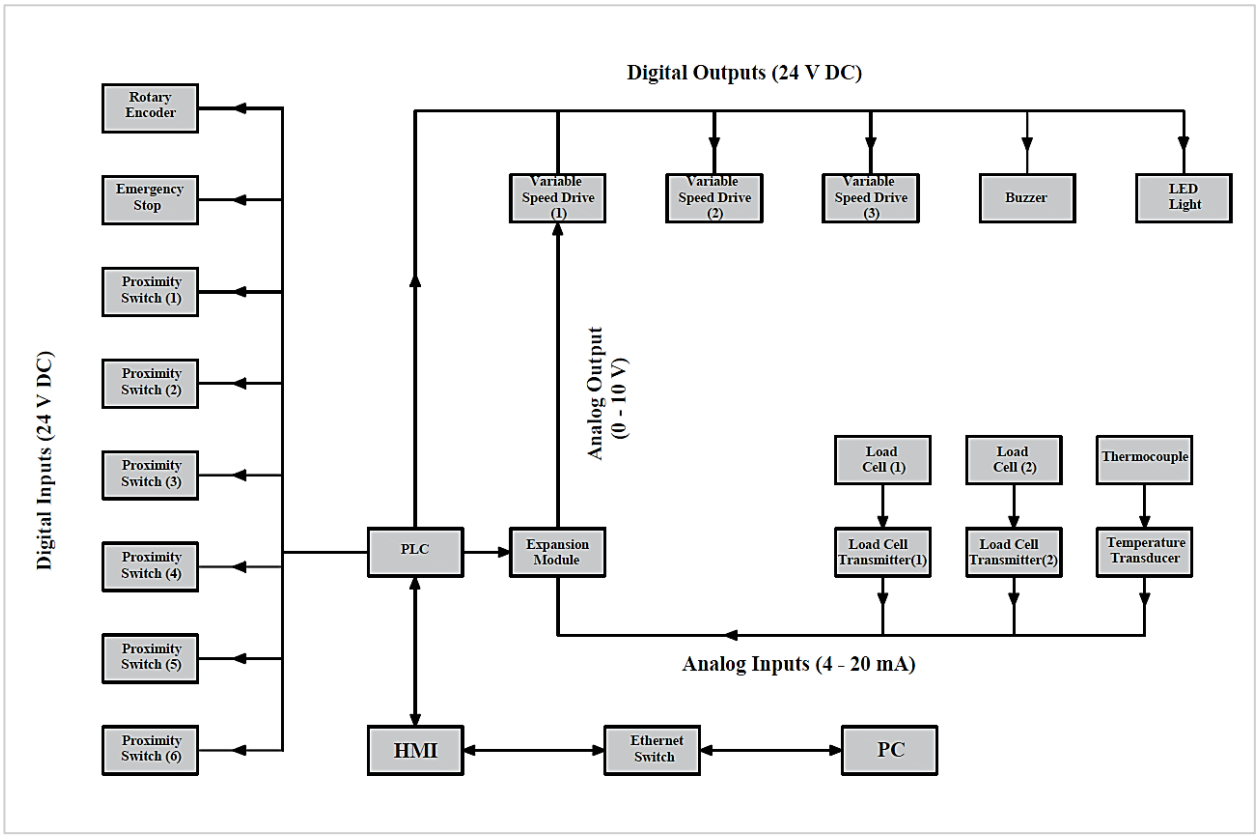

Figure 4: Block diagram of the control system using PLC

6.2 Hardware design of control system

Each component was selected carefully in the hardware design to fit the requirements and limitations. This model consists of Schneider PLC, expansion analog, network switches, and an HMI screen as shown in Figure 5. Each part of the control system mentioned above is discussed below:

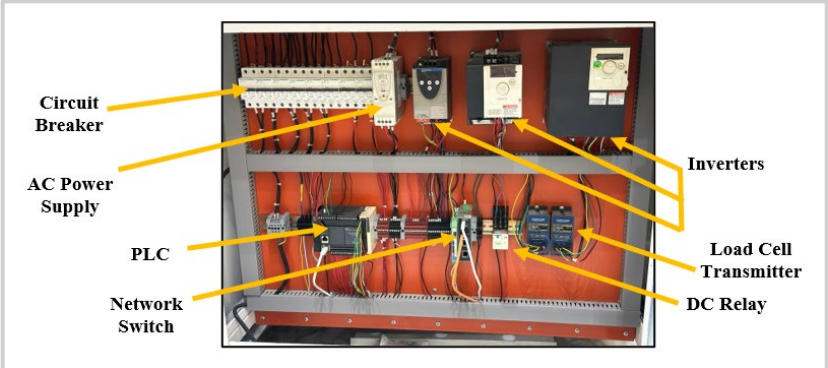

Figure 5: Hardware of the control system

6.2.1 Schneider PLC

The controller PLC used in this project is the Schneider TM221CE24T/TR/ OUT source/ 24 V DC. A logic controller can handle a broad range of applications and has many strong features, including 14 inputs (digital), 10 outputs (digital), and 2 inputs (analog).

6.2.2 Expansion module input and output (Analog)

The expansion, in Figure S4 as shown in the supplementary file, used in this work is the Schneider TM2AMM6HT/24 v dc. This part was used as needed for the input and output analog to program and control the wear parameters. It includes 4 inputs (analog), 2 outputs (analog)

6.2.3 Network switch

A network switch type Phoenix contacts automatic detection of data transmission, as shown in Figure S5 in the supplementary file, is a device that connects between PLC, HMI, and Personal Computer (PC) by using ethernet cables for

transferring programming commands (software programs) from the PLC to the HMI and vice versa, as well as this switch transfers programming commands (software programs) from the PC to the HMI.

6.2.4 Human machine interface (HMI)

One of the important parts of the programming system is the HMI touchscreen, which allows a user to interact with a device and enter the required data regarding wear test parameters to operate and control the machine [22]. This screen is an input for entering the required variables in each case and an output for controlling the PLC and executing instructions. Harmony Standard HMI GTO5310 is used in this work.

6.2.5 AC Induction motor

In this work, several types of three-phase induction motors were chosen to control the speed of the motors because variable speeds are needed in all motors. All motors were connected in a delta way to convert the voltage from 380 volts three-phase to 220 volts single-phase. Three induction motors were used, first for disc rotation and second for applying pressure to the pin to change the applied load. The first type of motor used in this work is the AC 3φ induction motor 2.2 kW, 220/380 V, 8.92 A, 50 Hz, 1420 rpm. This motor is responsible for the disc rotating at different speeds to test the wear rate of the sample.

The second type of motor used in pin-on-disc wear machine manufacturing is the AC 3φ induction motor 0.37 kW, 220/380 V, 1.84 A, 50 Hz, 1420 rpm. This type has a gearbox that increases the motor torque by decreasing the motor speed to control the motor's operation. The gearbox of this type has a capacity of 0.37 kW and a change ratio of 60/1, and it is responsible for the motor that changes the pressure value applied to the sample. Applying load is made possible by a toothed shaft by changing the pressure applied to the sample, as shown in Figure 6, which pushes the sample against the rotating disc. In this design, a new method was used to change the value of the applied load to the sample, which is the method of changing the applied pressure to the sample, unlike the previous method, which used variable value weights in each wear rate test. This method is achieved by using an AC induction motor with a teeth shaft, where the shaft applies pressure to the sample, and the load cell reads this pressure according to the required values programmed by a PLC program. When the pressure reaches the applied load required, the load cell gives a directive to the plc, and then the plc sends a signal to the AC drive to stop the motor from applying pressure to the sample. The second load cell measures the friction force generated between the disc and the sample to calculate the coefficient of friction (μ) for each metal and each case of the wear test parameters (rotating speed, applied load, applied time, and sliding distance). This is done by dividing the friction force generated between the rotating disc and the sample by the applied force to the sample according to Equation 4.

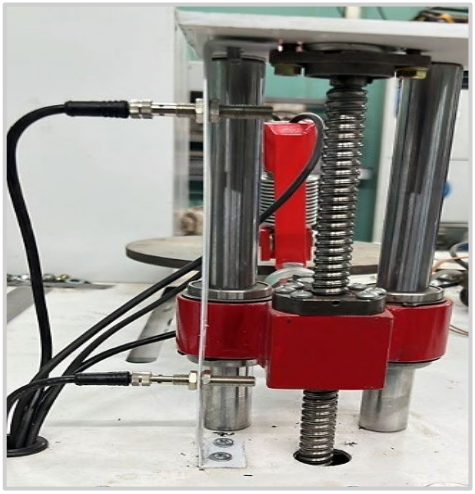

Figure 6: Three shafts for changing an applied load and the load cells fixing

6.3 Software design

Software design is an important part of the design of the PLC control system for pin-on-disc wear machines. When designing software, all kinds of situations in machines are considered. Four programs were installed on the personal computer to program and control the device. Schneider and Phoenix Company issued these programs. It includes So Move AC Drive Software used to program the variable speed drive, EcoStruxure machine expert-basic V1.2 VP1 Software is considered the basic software in programming the machine because it is related to PLC programming through the inputs (digital and analog) and the outputs (digital and analog), Vijeo designer 6.2 Software is for programming the HMI touchscreen, Ifs – Conf RTD Software is for programming the temperature transducer to measure the temperature in each wear test parameter as shown in Figures S6, S7, and S8 in the supplementary file.

6.4 Safety and protection devices

The emergency stop push button, proximity switch, and circuit breaker ensure the machine works correctly and is safe for the user.

6.5 Accessories

To complete the manufacturing of the pin-on-disc wear machine, Light Emitting Diode (LED) Light, Selector Switch, Buzzer, and DC Relay 24 V were added to provide ease of operation for the user, and these parts are explained below:

7. Results and discussion

7.1 Influence of applied load on the wear rate of AA 6061 alloy and CK45 steel alloy

The proposed algorithm and the parameters affected in this case are shown in Figure 7. Increasing the applied load increases the wear rate due to friction and the contact surface between the pin and disc. The applied load is affected by 85% at the wear rate owing to friction, and the temperature in the AA6061 alloy tests is greater than that of the CK45 steel alloy, as shown in Figure 8 a and b. As a result, the applied load will increase the wear rate [23, 24]. The wear rate value for AA6061 alloy is 3.2887 $x10^{-5}$gm/cm at (5 N) load and increases with increasing the applied load to 11.7403 $x10^{-5}$ gm/cm when the applied load is 25 N. For CK45 steel alloy, the wear rate value is 1.4094 $x10^{-5}$gm/cm at (5 N) load and increases with the applied load to 9.8701 $x10^{-5}$ at (25 N), the wear rate in the AA6061 alloy tests is greater than in the CK45 steel alloy. Figure 9 illustrates the relationship between applied load and wear rate at a constant rotating speed (300 rpm), sliding distance is 3 cm, sliding time is 5 min, and the range of applied load range is (5 – 25 N).

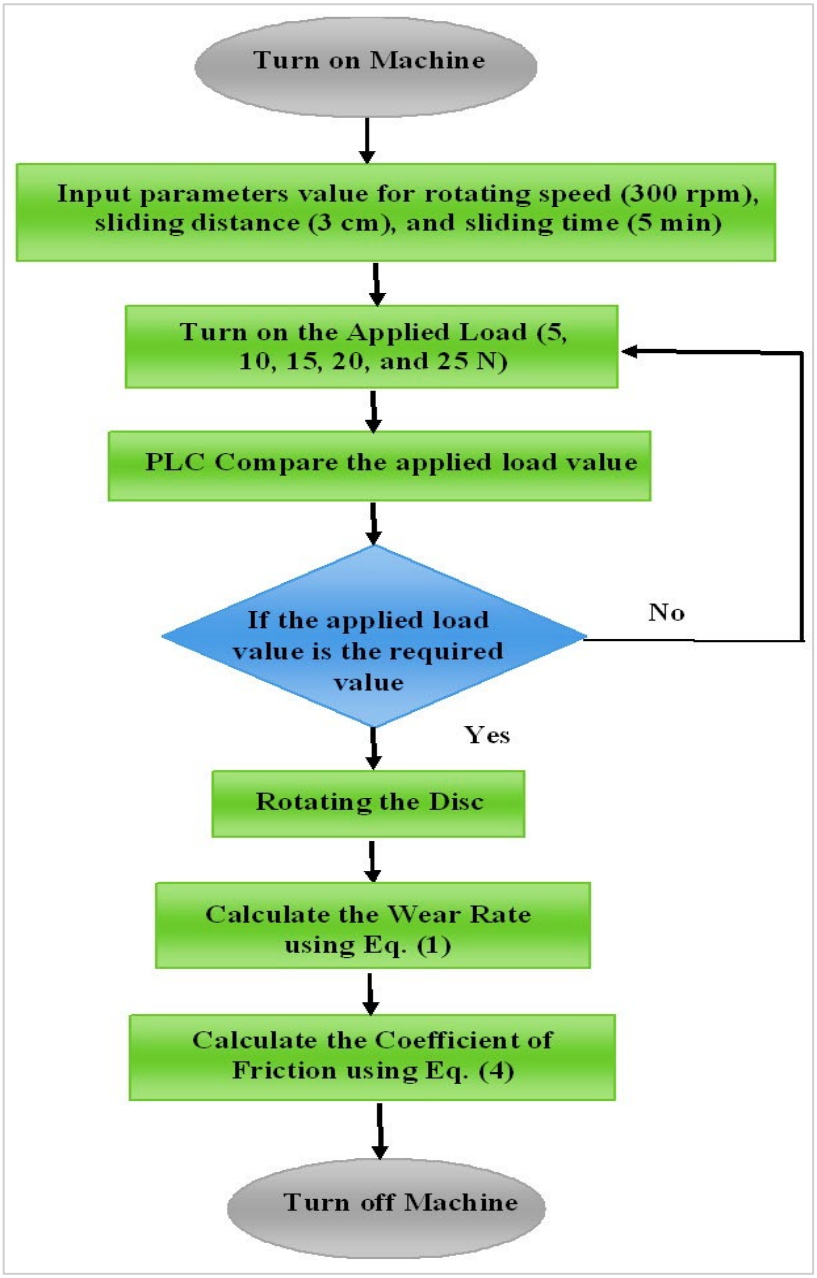

Figure 7: Flow chart represent the effect of the applied load on the wear rate of AA6061alloy and CK45 steel alloys

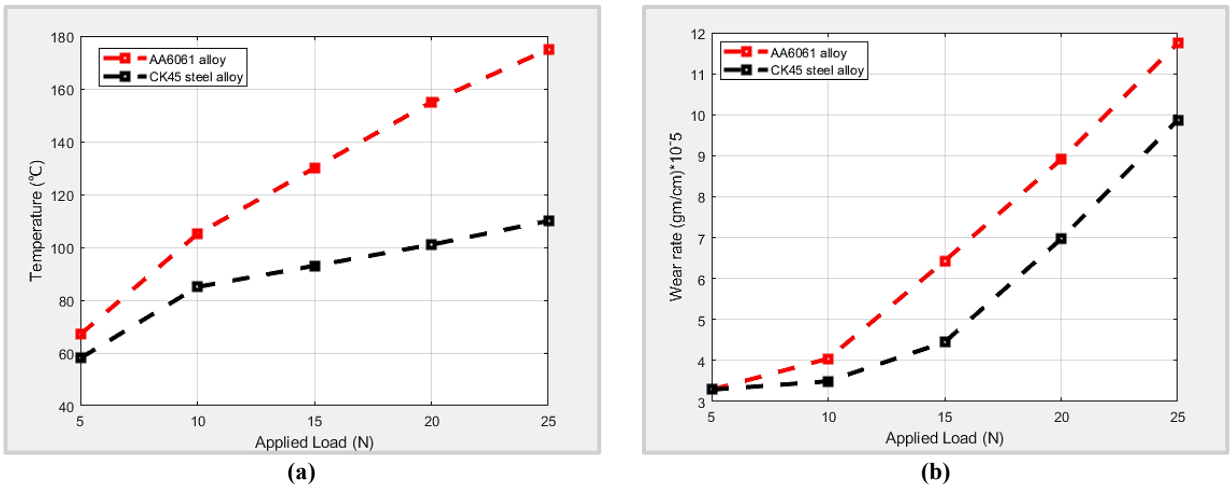

(a) **(b)**

Figure 8: The applied load for AA 6061 alloy and CK45 steel alloy: (a) vs. temperature (b) vs. wear rate

7.2 Influence of the applied load on the COF of AA 6061 alloy and CK45 steel alloy

Figure 9 demonstrates how a rise in the normal load caused a decrease in the coefficient of friction. Increased load on the sample resulted in compression and a comparatively flattened surface, which decreased the friction coefficient [25]. The generation of a continuous oxide film on the friction surface effectively avoided direct metal-to-metal contact between the friction pairs and reduced the occurrence of adhesive wear. This is mainly because when the pulsed current was passed into the metal during the process, the current easily produced an oxide layer on the aluminum alloy surface, and the current improved the oxidation properties of the sliding surface through surface polarity. The increased temperature effect of the pulsed current on the metal and the heat from the friction process also made the aluminum alloy surface more susceptible to oxidation. In contrast, the friction coefficient gradually decreased [26]. For AA6061 alloy, the C.O.F value is 0.6867 and decreased with increased applied load to 0.5886. For CK45 steel alloy, the C.O.F value is 0.5493 and decreased with increased applied load to 0.3727. Therefore, the AA6061 alloy coefficient of friction is more than the CK45 steel alloy coefficient of friction.

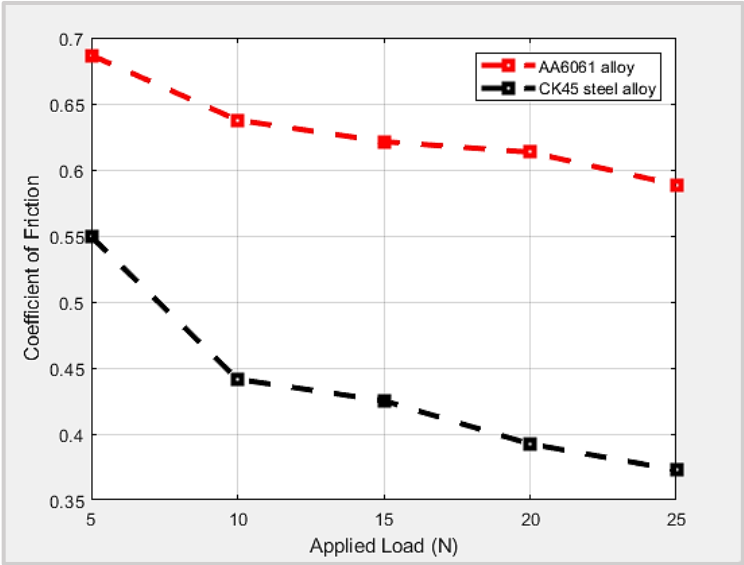

Figure 9: The applied load vs COF for AA 6061 alloy and CK45 steel alloy

7.3 Effect of rotating speed on the wear rate of AA6061

The proposed algorithm and the parameters affected by this case are shown in Figure 10. Increasing the rotating speed leads to minimizing wear rate owing to increasing the temperature at the surface where the pin and rotating disc make contact, as seen in Figure 11a. As a result of the increasing friction between them. Increasing the temperature between two contact surfaces will lead to the transmission of the material from one of them to another and create an oxidation layer, which minimizes the wear rate. The heat dissipation for higher rotating Speeds is lower than for lower rotating Speeds and, in turn, leads to the softening of asperities and minimizes the loads required to shear the welded points. Hence, the wear rate will be reduced [25,27]. In AA6061 and CK45 alloy, the temperature was 67 °C at (300 rpm) and increased with increasing the rotating speed. The temperature in the AA6061 alloy tests is greater than in the CK45 steel alloy. The wear rate is proportionately inverse to the change in rotating speed. The wear rate value for AA6061 alloy is 3.2887×10^{-5} gm/cm at (300 rpm) and decreases with increasing the rotating speed to 2.7979×10^{-5} gm/cm when the rotating speed is (900 rpm). For CK45 steel alloy, the wear rate

value is 1.4094 x10^{-5}gm/cm at (300 rpm) and decreases with increasing the rotating speed to 0.8678x10^{-5}gm/cm at (900 rpm). Figure 11b shows the rotating speed and wear rate relationship. In this instance, the sliding distance range is 3 cm, the applied load is 5 N, the rotation speed ranges from (300 – 900 rpm), and the sliding time is 5 minutes.

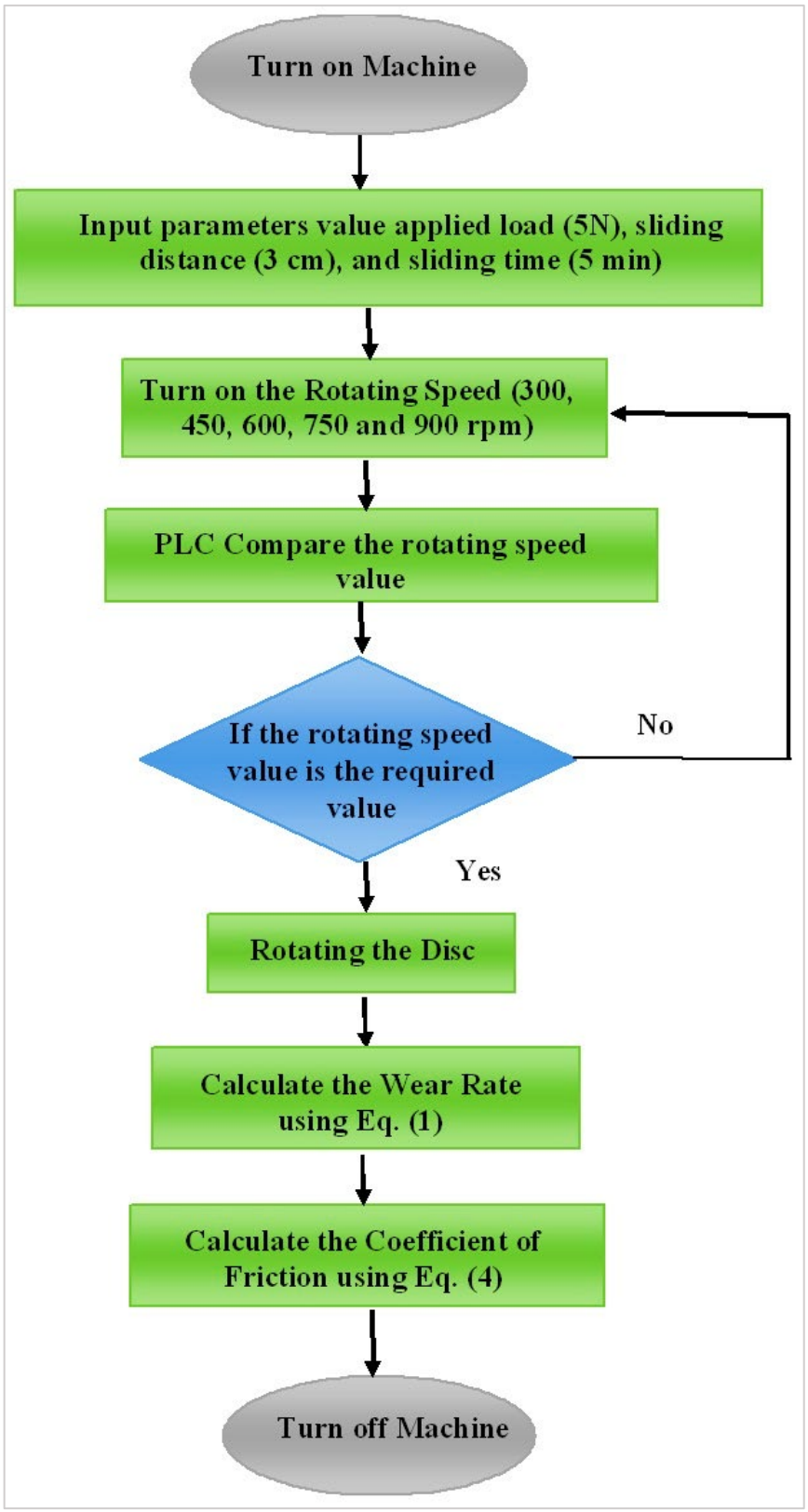

Figure 10: Flow chart represented the effect of the rotating speed on the wear rate of AA 6061 alloy and CK45 steel alloys

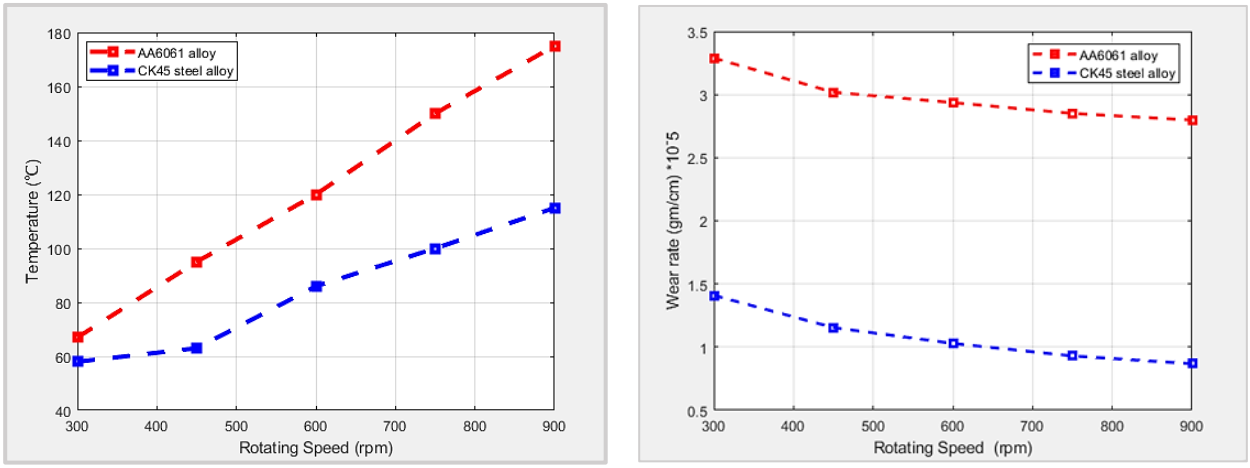

(a) **(b)**

Figure 11: The rotating Speed for AA 6061 alloy and CK45 steel alloy: (a) vs. temperature (b) vs. wear rate

7.4 Influence of the rotating Speed on the coefficient of friction

The highest rotating speed values were found to have the highest friction coefficient. As seen in Figure 12, the differences in friction coefficient levels under dry sliding conditions can be understood as a temperature rise in the steel surface brought on by frictional power. This leads to the weakening the bond and loosening of the alloy atomic chains. Consequently, the bonds break into pieces and create debris, increasing the coefficient of friction [25].

For AA6061 alloy, the C.O.F value is 0.6867 and increased with increased rotating speed to 0.7848. For CK45 steel alloy, the C.O.F value is 0.5493 and increased with increased rotating speed to 0.5984, therefore, the AA6061 alloy coefficient of friction is more than CK45 steel alloy coefficient of friction.

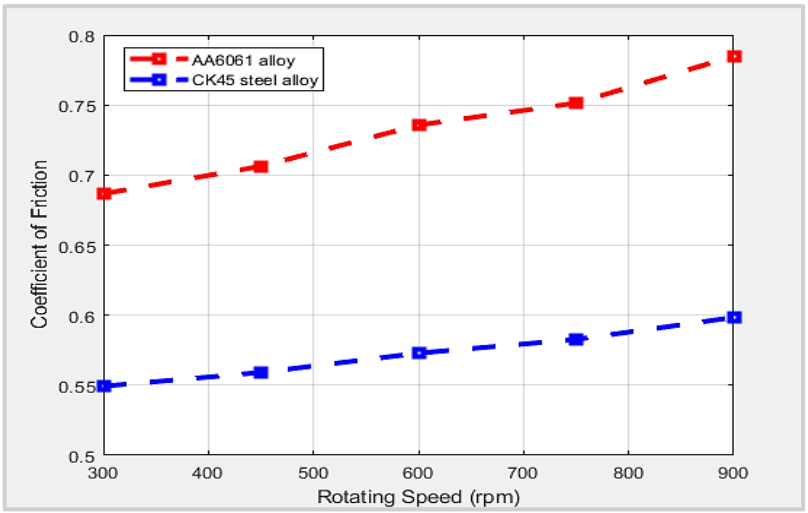

Figure 12: The rotating Speed vs. COF for AA6061 alloy and CK45 steel alloy

7.5 Effect of sliding time on the wear rate of AA 6061 and CK45 steel alloys

The proposed algorithm and the parameters affected in this case are shown in Figure 13. Increasing the sliding time will increase the contact time between the rotating disc and sample, increasing the temperature between two contact surfaces, as shown in Figure 14a. Owing to the increase in temperature at the contact surfaces, severe wear is created. Therefore, the wear rate affects the sliding time [23,27]. The wear rate value for AA6061 alloy is 3.2887×10^{-5} gm/cm and increased with increased the sliding time to 5.2083×10^{-5} gm/cm, for CK45 steel alloy the wear rate value is 1.4094×10^{-5}gm/cm and increased with increased the sliding time to 1.8820×10^{-5}gm/cm. Figure 14b explains the influence of increasing sliding time on the wear rate value, with sliding time ranging from (5 – 25 min). Another parameter is constant: the rotating speed is 300 rpm, the applied load is 5 N, and the sliding distance is 3 cm.

7.6 Influence of the sliding time on the COF of AA 6061 and CK45 steel alloys

Figure 15 demonstrates that a rise in sliding time caused a decrease in the coefficient of friction. A rise in sliding time resulted in compression and a relative flattening of the surface, decreasing the friction coefficient [27]. As the friction time gets longer, the friction depth increases. This implies a larger contact area between the AA6061 alloy and CK45 steel alloy and the

disc, inducing larger variation ranges for the friction force (Ft) and the applied load (Fn). Moreover, both the friction coefficient and the two forces (Fn and Ft) change periodically with the sliding time [28]. For AA6061 alloy, the C.O.F value is 0.6867 and decreased with increased sliding time to 0.5199. For CK45 steel alloy, the C.O.F value is 0.5493 and decreased with increased sliding time to 0.3598; therefore, the AA6061 alloy coefficient of friction more than the CK45 steel alloy coefficient of friction.

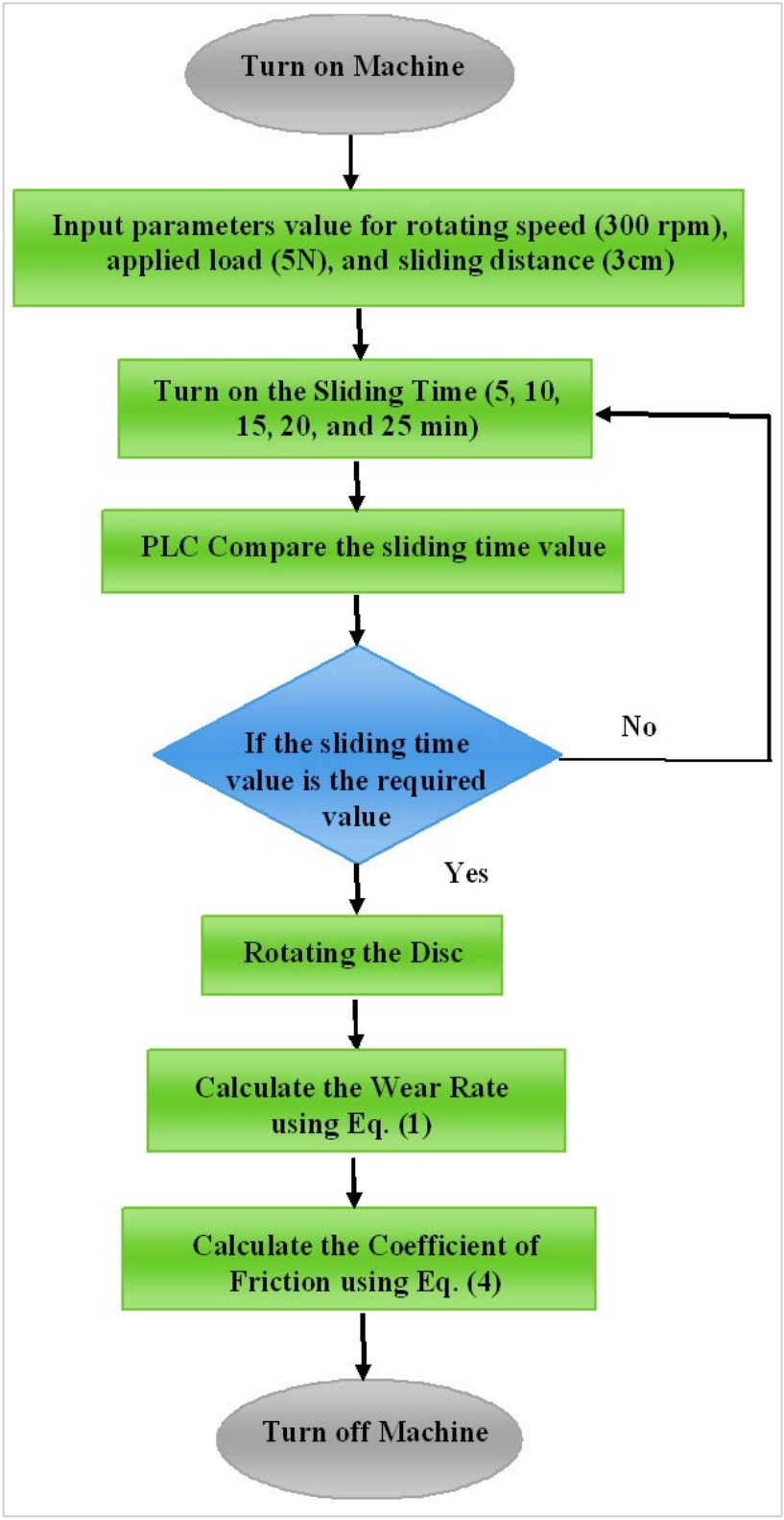

Figure 13: Flow chart of influence of sliding time on the wear rate of AA 6061 alloy and CK45 steel alloy

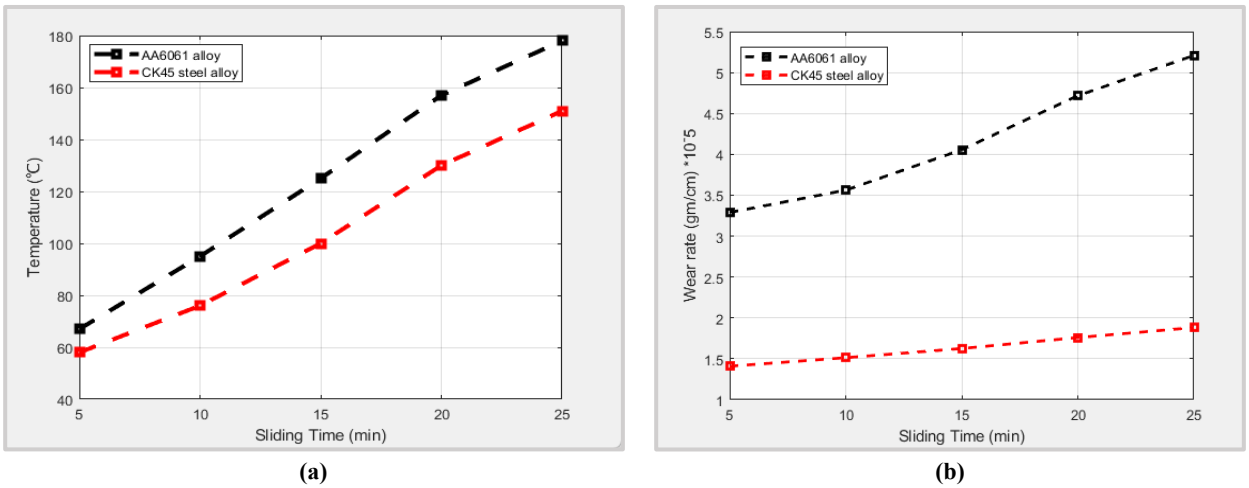

Figure 14: The sliding Time for AA 6061alloy and CK45 steel alloy: (a) vs. temperature (b) vs. wear rate

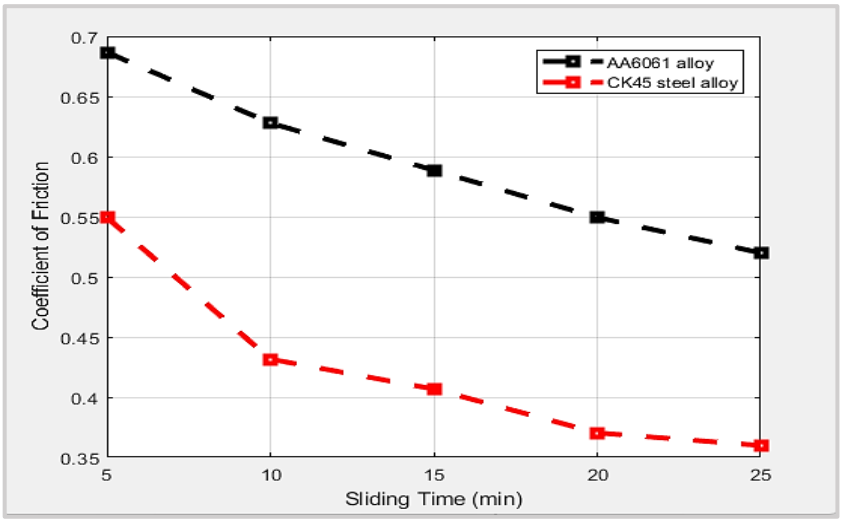

Figure 15: The sliding Time vs. COF for AA 6061 alloy and CK45 steel alloy

8. Conclusion

Depending on the results obtained through the PLC, changing the wear parameters became easier and more accurate in the results obtained by 25%. The use of the PLC programming system was very successful in controlling the operation of the three motors in terms of controlling the disc rotation speed, the load applied to the sample, and changing the distance between the disc center and the sample center to obtain different sliding distances, as well as controlling the sliding Time. Using the HMI screen and programming it with a PLC system led to the machine being programmed so that the user could enter the required data through the touch screen, obtain the outputs, and continuously monitor the device's performance through the graphics on the screen, which led to the ease of conducting tests on metal alloys and changing several parameters by the user, unlike other wear machines in which the user is forced to change the parameters affecting the wear rate every time manually. For AA6061 and CK45 alloys, the COF value increases with increased applied load, and the AA6061 alloy coefficient of friction is greater than the CK45 steel alloy coefficient of friction. The wear rate in the AA6061 alloy tests is greater than in the CK45 steel alloy. For AA6061 and CK45 alloy, the COF value increases with increasing rotating speed. The AA6061 alloy coefficient of friction is more than the CK45 steel alloy coefficient of friction. The wear rate in the AA6061 alloy tests is greater than that of the CK45 steel alloy. For AA6061 and CK45 alloy, the COF value is decreased with increased sliding time, and the AA6061 alloy coefficient of friction is more than the CK45 steel alloy coefficient of friction.

Author contributions

Conceptualization, K. Salman and A. Reja; data curation, H. Mohammed; formal analysis, H. Mohammed**,** K. Salman and A. Reja; investigation, H. Mohammed; methodology, H. Mohammed; project administration, H. Mohammed; resources, H. Mohammed; software, H. Mohammed; supervision, K. Salman and A. Reja; validation, K. Salman and A. Reja; visualization, K. Salman and A. Reja; writing—original draft preparation, H. Mohammed; writing—review and editing, K. Salman and A. Reja. All authors have read and agreed to the published version of the manuscript.

Funding

This research received no specific grant from any funding agency in the public, commercial, or not-for-profit sectors.

Data availability statement

The data that support the findings of this study are available on request from the corresponding author.

Conflicts of interest

The authors declare that there is no conflict of interest.

References

[1] Patnaik, A. , Singh, T. , Kukshal, V. Tribology in Materials and Manufacturing - Wear Friction and Lubrication; BoD–Books on Demand, 2021. https://doi.org/10.5772/intechopen.87674

[2] M. Hoi'c, A. Miklik, M. Kostelac, J. Deur, and A. Tissot, Analysis of the Accuracy of Mass Difference-Based Measurement of Dry Clutch Friction Material Wear, Materials, 14 (2021) 5356-5373. https://doi.org/10.3390/ma14185356

[3] V. Cortes, C. A. Rodriguez, J. A. Ortega, and H. Huq, Multidirectional Pin-on-Disk Testing Device to Evaluate the Cross-Shear Effect on the Wear of Biocompatible Materials, Instruments, 3 (2019) 35. https://doi.org/10.3390/instruments3030035

[4] Rupniewski, J. J. Evaluation of Linear Force Actuators in a Pin-on-Disc Test Rig Application. M.Sc. Thesis, KTH Royal University, 2020.

[5] Ch. Lazaridis, Design and FEA Study of a Novel Modular Multi-Functional Tribological Laboratory Test Rig. Diploma Thesis, National Technical University of Athens, 2021. http://dx.doi.org/10.26240/heal.ntua.22446

[6] M. Federici, G. Straffelini, and S. Gialanella, Pin-on-Disc Testing of Low-Metallic Friction Material Sliding Against HVOF Coated Cast Iron: Modelling of the Contact Temperature Evolution, Tribol. Lett. J., 4 (2017) 65-121. https://doi.org/10.1007/s11249-017-0904-y

[7] Sobarad, P. M. , Budihal, K. S. , Tripalgouda G., and Naik, P. K. Design and Fabrication of Wear Machine, Visvesv Araya Technology University, 2019.

[8] Carlos Felipe Ferreira Galvão, Guido Alves Slavec, Pedro Lucas De Araujo Menardi, Aparecido Carlos Gonçalves, Fábio Roberto Chavarette, Design and Construction of a Pin-On-Disk Experimental Bench to Determine The Friction Coefficients of Materials, Conference: 25th ABCM International Congress of Mechanical Engineering, 2021.

[9] H. M. Ali, Design and Manufacturing of a Pin-on-Disc wear Testing Apparatus, Kirkuk U. J. Sci. Studies, 12 (2017) 65-97. http://dx.doi.org/10.32894/kujss.2017.132385

[10] Shebani, A. Prediction of Wheel and Rail Wear Using Artificial Neural Networks. Ph.D. Thesis, University of Huddersfield, 2016.

[11] Rudnytskyj, A. Simulations of Contact Mechanics and Wear of Linearly Reciprocating Block-on-Flat Sliding Test. M.Sc. Thesis, University of Technology Department of Engineering Sciences and Mathematics, 2018.

[12] M. J. Valdes, Juan Gonzalo Ardila Marín, M.A. Rodriguez-Cabal, and J.D. Betancur, Tribometry: How is Friction Research Quantified? A Review, Int. J. Eng. Res. Technol., 13 (2020) 2596-2610. http://dx.doi.org/10.37624/IJERT/13.10.2020.2596-26104

[13] M. Federici, G. Straffelini, and S. Gialanella, Pin-on-Disc Testing of Low-Metallic Friction Material Sliding Against HVOF Coated Cast Iron: Modelling of the Contact Temperature Evolution, Tribol Lett J., 4 (2017) 65-121. https://link.springer.com/article/10.1007/s11249-017-0904-y

[14] Martin, S. Study of the Wear Behavior of SS16L + WC Composites: Role of the Counter. M.Sc. Thesis, de Liège University, 2020.

[15] Maroš Kováč, Bc. Multi-Speed Gearbox for Passenger EV. M.Sc. Thesis, Czech Technical University, 2021.

[16] W. Chang, J. Xie, J.Wang, W. Teng, Y. Sun1 and M. Zheng, Application of PLC and HMI in the measurement and control platform of single-tube heat transfer experiment rig, Adv. Mech. Eng. J., 12 (2020) 1-14. http://dx.doi.org/10.1177/1687814020971162

[17] M. S. Hamza Al-Radhi, S. J. Dawood Al-Kamil and S. Tamás, A model-based machine learning to develop a PLC control system for Rumaila degassing stations, J. Pet. Res. & Studies, 12 (2020) http://dx.doi.org/10.1177/1687814020971162

[18] A. L. Saleh, L. F. Naeem, and M. J. Mohammed, PLC Based Automatic Liquid Filling System For Different Sized Bottles, Int. Res. J. Eng. Technol., 4 (2017) 57-61.

[19] Chithadka, S. A PLC-Based Real-Time Material Flow Controller/Calculator in Warehouse Management System. M.Sc. Thesis, Technische University, 2018.

[20] Shekasteh, M. Automation and PLC-HMI Programming & Configuration. M.Sc. Thesis, Politecnico di Torino University, 2020.

[21] M. S. Saleh, Kh. G. Mohammed, Z. S. Al-Sagar, A. Z.Sameen, Design and Implementation of PLC-Based Monitoring and Sequence Controller System, J. Adv. Res. Dyn. Control Syst., 10 (2018) 2281-2288.

[22] N. Idusuyi, and J. I. Olayinka, Dry Sliding Wear Characteristics of Aluminum Metal Matrix Composites, J. Mater. Res. Technol., 8 (2019) 3338-3346, https://doi.org/10.1016/j.jmrt.2019.04.017

[23] S. V. Wagh, Dh. V. Bhatt, J. V. Menghani, and Sh. S. Bhavikatti, Effects of Laser Hardening Process Parameters on The Mechanical and Wear Properties of CK45 Steel Using an Orthogonal Array, Int. J. Mod. Manuf. Technol., 10 (2018) 86-93.

[24] J. Y. Byun, N. N. Okechukwu, E. Lee, J. G. Park, and W. Choi, Friction Characteristics of Aluminized Polyester Fabric under Dry and Water- Lubricated Conditions, Tribol. Lubr. J., 35 (2019) 396-402. https://doi.org/10.9725/kts.2019.35.6.396

[25] N. Radhika, and R. Raghu, Influence of Parameters on Sliding Wear of Titanium Nitride Coated 6061 Aluminum Alloy, Faculty Eng., 40 (2018) 203-212. http://dx.doi.org/10.24874/ti.2018.40.02.04

[26] J. Xia, R. Liu, J. Zhao, Y. Guan and Sh. Dou, Study on Friction Characteristics of AA7075 Aluminum Alloy under Pulse Current-Assisted Hot Stamping, Metals, 13 (2023) 972-991. https://doi.org/10.3390/met13050972

[27] B. S. Ravindranath, B. R. Murthy, H. C. Ramu and S. S. Nambiar, Process Parameters Optimization of Pin-on-Disc Wear Test to Minimize the Wear Loss of General-Purpose Aluminum Grades by Taguchi and Simulation through Response Surface Methodology, Eng. Sci., 16 (2021) 366-373. http://dx.doi.org/10.30919/es8d597

[28] H. Wang, T. Zhang, S. Wang, and Suet To, Characterization of the Friction Coefficient of Aluminum Alloy 6061 in Ultra-Precision Machining, Metals, 10 (2020) 366-348. https://doi.org/10.3390/met10030336